RSC Advances

PAPER

View Article Online
View Journal | View Issue

Cite this: *RSC Adv.*, 2021, **11**, 1001

Facile fabrication of a Janus mesh for water fluid unidirectional transportation†

Ziqi Li, Weitao Liang, * Weiping Li, Ze Wang, Liqun Zhu, Haining Chen and Huicong Liu *

A Janus membrane/mesh is a type of functional membrane/mesh composed of opposing wetting properties formed into a single layer in order to achieve novel properties. Janus membranes/meshes have attracted increasing attention from materials scientists due to their promising applications in the fields of microfluid transportation, water–oil separation and cleaning energy applications. Herein, we report a simple method to fabricate a Janus mesh by combining opposite wettability functions into one copper mesh substrate. The superhydrophilicity is achieved by chemical etching and the superhydrophobicity is fabricated by hydrophobic SiO_2 nanoparticle spraying. Due to its special composition and structure, the prepared mesh demonstrates distinct wetting properties on its two sides. Meanwhile, aqueous fluids can pass through the mesh from the hydrophobic side to the hydrophilic side spontaneously, whilst being blocked by the mesh when coming from the other direction. This unique property can realize unidirectional transportation of water fluids. The mechanism of the unique property based on Janus wettability is proposed and the stability of the prepared Janus mesh was also tested. The prepared Janus mesh can be used in the fields of microtidal energy, the chemical industry and in astronautics, demonstrating promising practical prospects.

Received 10th October 2020
Accepted 20th November 2020

DOI: 10.1039/d0ra08632k

rsc.li/rsc-advances

1. Introduction

Materials with superwettability have attracted the attention of researchers due to their unique chemical and physics properties as well as their extensive practical prospects.[1–4] In previous studies, researchers have found that superhydrophobic materials can be utilized in the fields of antifouling surfaces[5–7] and water droplet controlling,[8] while superhydrophilic materials can be used in the fields of fog harvesting[9–11] and in the chemical industry.[12] Recently, it has been found that a membrane/mesh with binary wettability, and is fabricated by combining hydrophilicity and hydrophobicity into one membrane/mesh, can achieve novel properties.[13–15]

Janus was an ancient Roman god with two different faces. The Janus membrane/mesh obtained this interesting name due to its asymmetric composition with regards to its wettability.[13] Scientists combined opposite properties into one membrane/mesh and collectively named it as a "Janus membrane/mesh". Amongst all types of Janus membranes/meshes, the combination of hydrophilicity and hydrophobicity is the most studied property. A Janus membrane/mesh has plenty of unique properties due to its binary wettability and porous structure. This type of membrane/mesh has promising prospects in the fields of oil/water separation,[16–25] microfluidic transportation,[3,13] demulsification,[26–29] and so on.[30] The behavior of water is mostly affected by interface tension when it comes into contact with the mesh surface.[1] However, the Laplace pressure that is generated at the interface influences the behavior of water in the pores.[13] The Laplace pressure that is generated by the interface can be calculated from the well-known Laplace equation:

$$\Delta p = \frac{2\gamma}{R} \quad (1)$$

where Δp is the Laplace pressure, γ is the surface tension of the interface and R is the radius of the curvature of the interface.

Water can maintain a stable shape on two sides of traditional hydrophilic surfaces or hydrophobic surfaces.[1] However, for a Janus mesh, the asymmetric wettability can cause distinct surface tensions on two sides of the mesh. When waterflow penetrates the mesh and enters the pores, the interface of the water can generate different Laplace pressures on the two sides of the mesh. The changes in Laplace pressure can influence the water, causing distinctive wetting behavior and achieving novel functions.[13] This type of mesh has promising prospects in the fields of oil/water separation,[16–25] microfluidic transportation,[3,13] demulsification[26–29] and so on.[30] Due to their unique properties and extensive practical prospects, Janus

Key Laboratory of Aerospace Materials and Performance (Ministry of Education), School of Materials Science and Engineering, Beihang University, Beijing 100191, China. E-mail: lwt@buaa.edu.cn; liuhc@buaa.edu.cn; Fax: +86 1082317113; Tel: +86 1082317113

† Electronic supplementary information (ESI) available. See DOI: 10.1039/d0ra08632k

meshes have attracted the attention of materials scientists on a global scale.

In previous work, scientists have studied methods of Janus membrane/mesh fabrication and have conducted much explorative research. The most studied property of a Janus membrane/mesh is water/oil separation. Yao fabricated a double-woven structure Janus membrane with hydrophobic yarns on one side and hydrophilic yarns on the other side.[25] The water contact angle on the hydrophobic surface was 152.8 ± 0.3°, and the contact angle on the hydrophilic side was almost 0° (water droplets were absorbed immediately by the membrane). The water droplets can penetrate the woven membrane from the hydrophobic to the hydrophilic side, whilst being blocked in the opposite direction. This phenomenon demonstrates the potential of the unidirectional water transporting property of a Janus membrane. The double woven system can be used for water/oil separation. Lin fabricated a Janus mesh on a stainless steel mesh substrate.[16] In the study, an acid solution was used to etch the mesh, endowing it with hydrophilicity. Then, hydrophobic particles were deposited onto one side of the mesh. The water contact angle of the hydrophobic side was 164 ± 0.5°, and the contact angle of the hydrophilic surface was almost 0°. Interestingly, the mesh showed oleophilicity on the hydrophobic side and oleophobicity on the hydrophilic side. This type of Janus wetting system can also be utilized in water/oil separation processes. The mesh showed excellent water/oil separation ability. Liang used electro-spun technology to fabricate a Janus membrane.[24] In the experiment, an electro-spun PS nanofiber demonstrated hydrophobicity while the electro-spun PAN nanofiber was hydrophilic. The contact angle of the hydrophobic PS membrane was 126 ± 0.2°. The electrospun Janus membrane showed outstanding demulsification ability and had a promising prospect in oil leaking situations. However, there are many drawbacks in the fabrication of these mentioned Janus membranes, such as a high fabricating expense, a complex preparation process, poor stability, and so on, and this greatly limits their practical application. It is therefore necessary to develop a simple and inexpensive method of constructing a stable Janus mesh.

Our group has extensive experience in preparing superwetting materials.[31–36] In our previous work, several substrates with a special wetting property have been prepared and excellent performance of these substrates was achieved. In this work, we report a novel method to fabricate a new type of Janus mesh. We sprayed hydrophobic modified SiO_2 nanoparticles onto one side of the mesh for hydrophobic modification.[37,38] To fabricate the hydrophilic property on the mesh, we soaked the mesh into potassium persulfate solution, endowing the surface with hydrophilicity.[39,40] The water contact angle of the hydrophobic mesh that was fabricated by the spraying method was tested to be 162 ± 0.4°, and the water contact angle of the hydrophilic mesh that was treated by the etching process was less than 5°. The influence of mesh numbers on the surface wetting behavior was also studied. We found that a Janus mesh with a mesh number of 200 demonstrated the best wetting property. In order to combine the two opposite wetting properties, the mesh was floated on the interface of the potassium persulfate solution so that the hydrophobic side could be kept upwards without etching by the solution. The unidirectional water transportation property was studied in a mimic glass tube. The prepared Janus mesh could block the transport of water fluid in the hydrophilic-to-hydrophobic direction. Meanwhile, the water fluid could pass through the mesh from the hydrophobic side to the hydrophilic side. The mesh also presented excellent stability. A mechanism, based on the superwetting theory, was also proposed to explain the unique property. The unidirectional water transportation property shows wide application prospects in the energy industry and in vessel surgery.

2. Experimental

2.1 Materials

Brass meshes (copper: 64 wt%, zinc: 36 wt%) (mesh number: 50, 100, 200, 300) were used as the substrates. KOH and $K_2S_2O_8$ were purchased from Xilong (AR, China), and absolute ethanol and nano SiO_2 particles were purchased from Beijing Chemical works (AR, China). The sizes of the corresponding mesh numbers are shown in Table 1.

2.2 Preparation

2.2.1 Copper substrate preparation. In order to remove the dirt and oxides from the commercial copper mesh, the mesh was first immersed in ethanol and rinsed in an ultrasonic cleaner. It was then rinsed with deionized water. Sulfuric acid solution (0.1 mol L^{-1}) was prepared and the mesh was immersed in the solution for a few seconds to remove the oxides. Finally, the mesh was taken out of the solution and was rinsed with deionized water before drying.

2.2.2 Hydrophobic modification of one side by SiO_2 nanoparticle spraying. 5 g of SiO_2 nanoparticles and 100 ml of absolute ethanol were prepared, and this solution was rinsed by ultrasonication for 20 min. 2 ml of OTS was added and the mixture was kept at 40 °C with magnetic stirring for 1 h. The hydrophobic modified SiO_2 nanoparticles were filtered and washed with absolute ethanol. The process was repeated and the nanoparticles were dried. Finally, the hydrophobic modified SiO_2 nanoparticles were successfully prepared. 3 g of the as-prepared SiO_2 nanoparticles was taken and dissolved in 50 ml of absolute ethanol, and then was ultra-sonicated for 20 min after magnetic stirring for 5 min. One surface of the copper mesh was sprayed with the solution 4 times, and was then dried in an electrothermal blast dryer at 80 °C for 5 min. The process was repeated 5 times. After the process, one side of the mesh became hydrophobic.

Table 1 The sizes of corresponding mesh numbers

Mesh number	Size of lattice
50	0.300 mm
100	0.150 mm
200	0.075 mm
300	0.050 mm

2.2.3 Fabrication of the hydrophilic properties. First, 4 g of potassium persulfate and 1.4 g of potassium hydroxide were prepared and were dissolved into 100 ml deionized water. Then, a Petri-dish was prepared with some of the above solution in it, and the mesh was placed carefully on the interface of the solution. The etching process took 10 min, and then the mesh was removed vertically so that the potassium persulfate solution did not splash onto the top of the mesh and affect the hydrophobic upward surface. The mesh was cleaned with deionized water and dried.

3. Results and discussion

3.1 Surface morphology and composition analysis

Fig. 1 demonstrates the morphologies and wetting behaviors of the meshes that were treated with different modifications. In this experiment, we utilized a brass mesh as a substrate. Fig. 1(a1) shows the SEM image of the bare substrate surface. From the image, we can see that the brass substrate is rather smooth, with some irregular crystalline grains on it. The results match well with the typical SEM images of a copper surface. Fig. 1(a2) shows the image of a water droplet in contact with the brass mesh substrate. In this image, the original mesh substrate shows low hydrophobicity and the water contact angle is about 100°. Fig. 1(b1) shows the SEM image of a copper mesh treated with the hydrophobic modification. A hydrophobically modified SiO_2 nanoparticle solution was sprayed onto the copper mesh to fabricate the superhydrophobic coating. The diameter of the SiO_2 particles was about 100 nm. The hydrophobic group of $-CH_3$ was introduced onto the modified nano-SiO_2 particle, so that the surface energy of the mesh reduced dramatically. At the same time, the nano-size SiO_2 particles could form

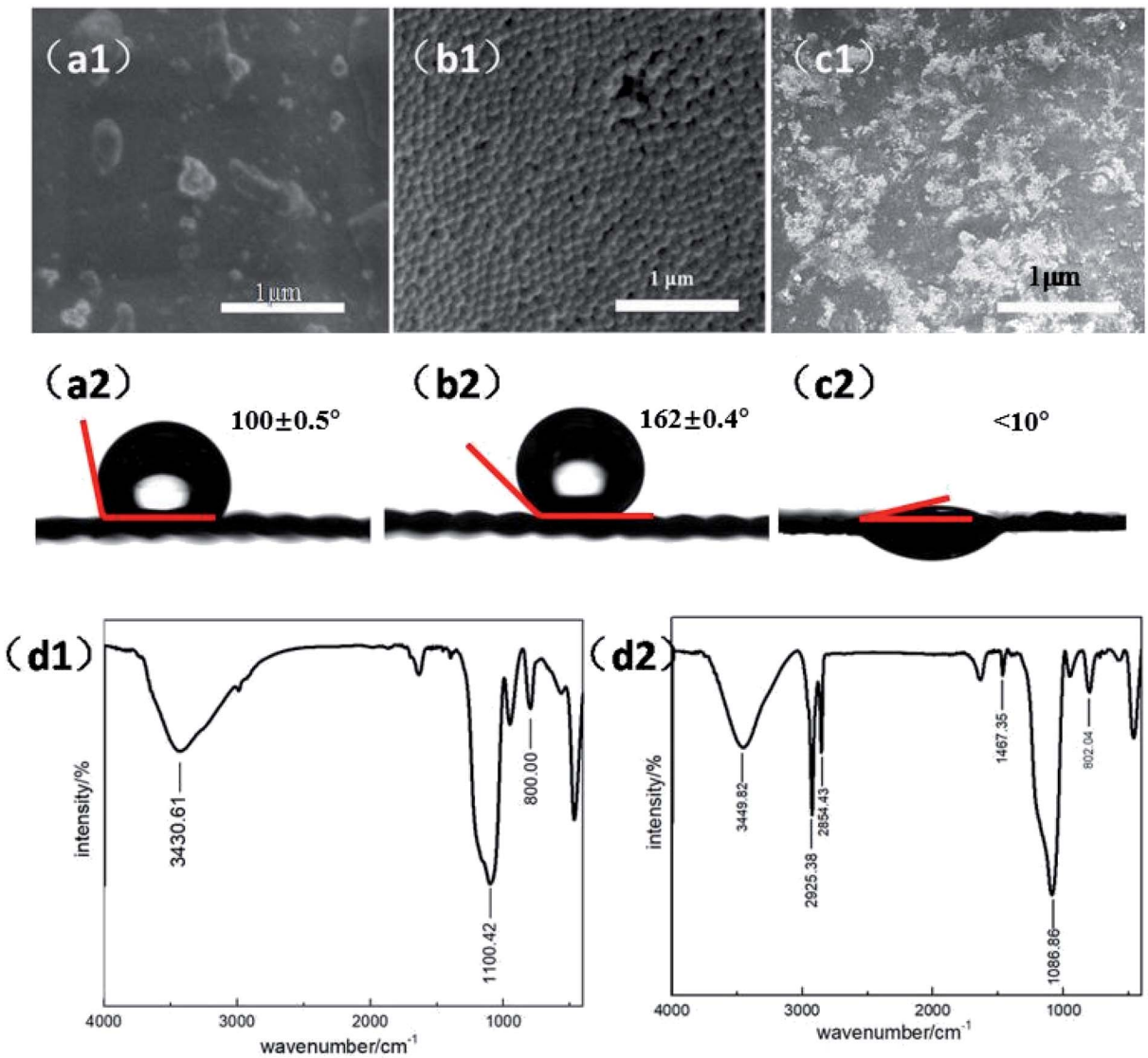

Fig. 1 Surface morphology, water contact angles and composition of three types of meshes. (a1), (b1) and (c1) Show the SEM images of the original substrate, the surface after the hydrophobic spraying process and the surface after the hydrophilic etching process, respectively. (a2), (b2) and (c2) Show the wetting behaviors of the original mesh substrate, the hydrophobic mesh and the hydrophilic mesh, respectively. (d1) and (d2) Are the infrared spectra of the mesh after the blank spraying process and the mesh after the hydrophobic spraying process, respectively.

a microstructure on the surface. According to the Wenzel equation, the relationship between the contact angle and surface tension can be described as follows:

$$\cos\theta = \frac{\gamma_{SG} - \gamma_{SL} \times r}{\gamma_{LG}} \quad (2)$$

where γ_{SG}, γ_{SL} and γ_{LG} stand for the surface tensions of the solid–gas interface, the solid–liquid interface and of the liquid–gas interface. r is a parameter that reflects the roughness of a surface ($r \geq 1$). From eqn (2), we can conclude that the roughness can enhance the hydrophilicity of a hydrophilic surface and can also enhance the hydrophobicity of a hydrophobic surface. Therefore, the microstructure that is formed by the nano SiO_2 particles can increase the hydrophobicity of the surface. As Fig. 1(b2) shows, the water contact angle of the sprayed mesh is about 162 ± 0.4°, demonstrating the superhydrophobicity of the as-prepared mesh. For the hydrophilic modification, we utilized the oxidizing effect of potassium persulfate solution and created a hydrophilic layer on the copper mesh substrate. The oxidizing process can generate copper oxide on the mesh and can increase its surface energy. The etching process can form a flower-like microstructure on the wire surface, and this is shown in Fig. 1(c1). This microstructure can increase the roughness and can also enhance the hydrophilicity of the surface according to eqn (2). Water droplets were absorbed onto the mesh immediately and the static water contact angle was less than 10°, as shown in Fig. 1(c2). A comparison of Fig. 1(c2) with Fig. 1(b2) indicates the great difference between the wetting behaviors of a hydrophilic mesh and a hydrophobic one. Fig. 1(d1) shows the infrared spectrum of the mesh treated with blank spraying, while Fig. 1(d2) shows the infrared spectrum of the mesh treated with hydrophobic spraying. There are obvious distinctions in the 2925 and 2854 cm^{-1} wavenumbers in Fig. 1(d2), and this matches well with the characteristic peaks of a $-CH_3$ group. The appearance of the $-CH_3$ group confirms that the hydrophobic modifier has been attached onto the substrate successfully.

3.2 Analysis of the gradient of the mesh numbers

The mesh number affects the wetting behavior of the mesh tremendously. In order to achieve the best unidirectional water transporting function, the influence of the mesh number is studied, and the result is shown in Fig. 2. In our experiment, four different mesh numbers (50, 100, 200, and 300) were chosen. Optical images of the meshes with different mesh numbers in the same field of vision are shown in Fig. 2(a)–(d). Fig. 2(a)–(d) show the optical images of the mesh substrates with different mesh numbers of 50, 100, 200 and 300, respectively. From the optical images, we can see that, in the same field of vision, the density of the holes increases with increasing mesh number. The water droplets also behave differently on the meshes with various mesh numbers. To determine the ideal mesh number of the substrate, we treated the meshes with the above-mentioned modification and tested their wettability. The water contact angles (WCAs) that were captured by the contact angle meter are shown. Fig. 2(a1)–(d1) show the WCA images of the hydrophobic meshes. In Fig. 2(a1), we can see that the water contact angle is about 100 ± 0.5°, and the specimen shows low hydrophobicity. However, in Fig. 2(b1)–(d1), the water contact angles clearly change when the mesh number increases to 100, 200 and 300. The contact angle of the specimen with a mesh number of 100 is about 145 ± 0.2°, and this can reach up to 162 ± 0.4° with mesh numbers of 200 and 300. The static contact angle results demonstrate the excellent hydrophobicity of the corresponding meshes. On the other hand, Fig. 2(a2)–(d2) show the images of the meshes etched by potassium persulfate, and all the meshes are hydrophilic. In Fig. 2(a2)–(c2), which are for the specimens with mesh numbers 50, 100 and 200, respectively, the contact angles are less than 10°. Therefore, water droplets can penetrate the mesh easily. The water contact angle increases to about 30 ± 0.6° when the mesh number increases to 300, as shown in Fig. 2(d2), and the water droplets can also pass through the mesh. The hydrophilicity of the mesh decreases with a mesh number of 300. Based on the above experiments, the substrate with a mesh number of 200

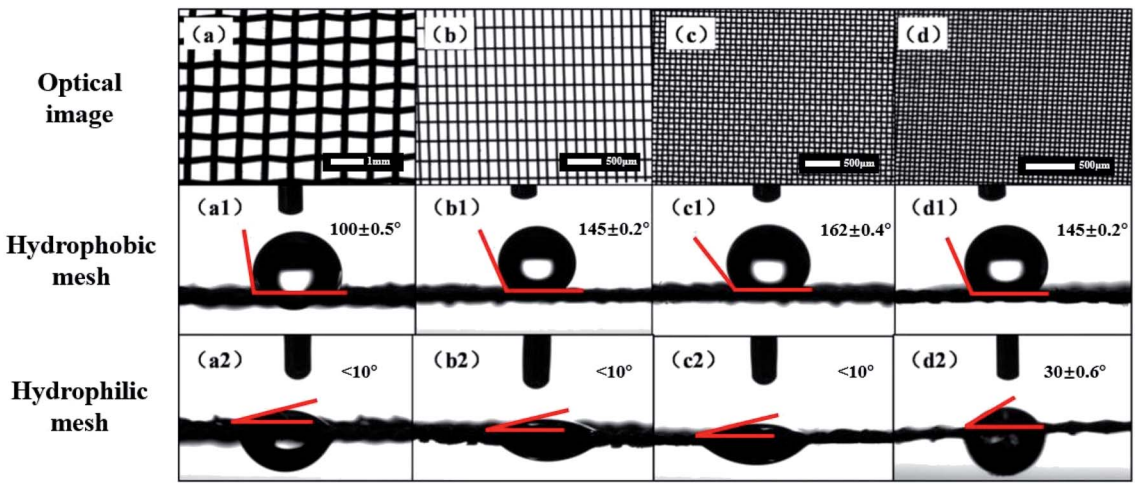

Fig. 2 Images regarding analysis of the gradient of the mesh numbers. (a) to (d) Are the optical images of the meshes with mesh numbers of 50, 100, 200 and 300. (a1) to (d1) Show the static water contact angles of hydrophilic meshes with corresponding mesh numbers, and (a2) to (d2) demonstrate the static water contact angles of the hydrophilic meshes with corresponding mesh numbers.

demonstrates the best wetting performance in terms of both hydrophilicity and hydrophobicity. Consequently, we chose the copper mesh with a mesh number of 200 as the substrate of the Janus mesh.

3.3 Wetting behavior analysis

In Fig. 1 and 2, the static wetting behavior of the prepared surface is demonstrated. In order to further observe the wetting behaviors of the prepared mesh, the dynamic contact process is captured by a contact angle meter and the results are shown in Fig. 3. The procedure for a water droplet coming into contact with the prepared hydrophobic mesh is demonstrated in Fig. 3(a1)–(f1). The black arrow represents the direction of movement of the mesh. Fig. 3(a1) and (b1) show that the mesh approaches the droplet and is then in contact with the droplet. The mesh keeps moving upwards and then squeezes the droplet, and this is shown in Fig. 3(c1). Afterwards, the mesh starts to move downwards. Fig. 3(d1) and (e1) show that the droplet has been drawn into a spindle-like shape by the hydrophobic mesh, instead of dropping on the surface. Finally, the water droplet detaches from the mesh, as shown in Fig. 3(f1). The droplet was pulled into a spindle-like shape by the surface of the mesh, and this shows the excellent hydrophobic property of the surface. Fig. 3(a2)–(f2) show the process of a water droplet in contact with a hydrophilic mesh. Using the same testing procedure as for the hydrophobic mesh, the hydrophilic mesh first moves upwards to be in contact with the droplet, and this is shown in Fig. 3(a2) and (b2). The water droplet was quickly absorbed by the mesh as soon as they came into contact, as shown in Fig. 3(c2). When the syringe was pulled away from the mesh, the droplet detached from the syringe and spread out onto the mesh spontaneously, as shown in Fig. 3(d2)–(f2). From this procedure, we found that the water droplet was absorbed by the mesh and spread immediately as soon as it came into contact with the hydrophilic surface, indicating the outstanding hydrophilicity of the oxidized mesh.

The spraying and etching treatments that are used in this work are two conventional modification methods that are used to generate different wettability effects on a surface.[37–40] However, the two methods cannot be conducted on one mesh simultaneously, in order to obtain their opposite effects. Due to the porous nature of meshes, the ingredients of the solution will inevitably infiltrate to the other side when spraying on one side. The spraying modification method finally fabricates a unified hydrophobic mesh. It is clear that immersing a mesh into potassium persulfate solution entirely will oxidize both sides of the mesh. In order to fabricate Janus wettability on one mesh substrate, the two methods must be effectively combined. In our experiment, we sprayed the hydrophobic SiO_2 nano particles on one side of the mesh first, then we floated the as-prepared mesh on the interface of potassium persulfate solution. The etching process can then endow the treated side with the hydrophilic property. At the same time, by remaining in the air phase, the sprayed modified side can be kept away from the liquid phase and maintain its hydrophobic property. Through the above-mentioned method, a Janus mesh with opposite wettability on different sides could be fabricated, as shown in Fig. 4.

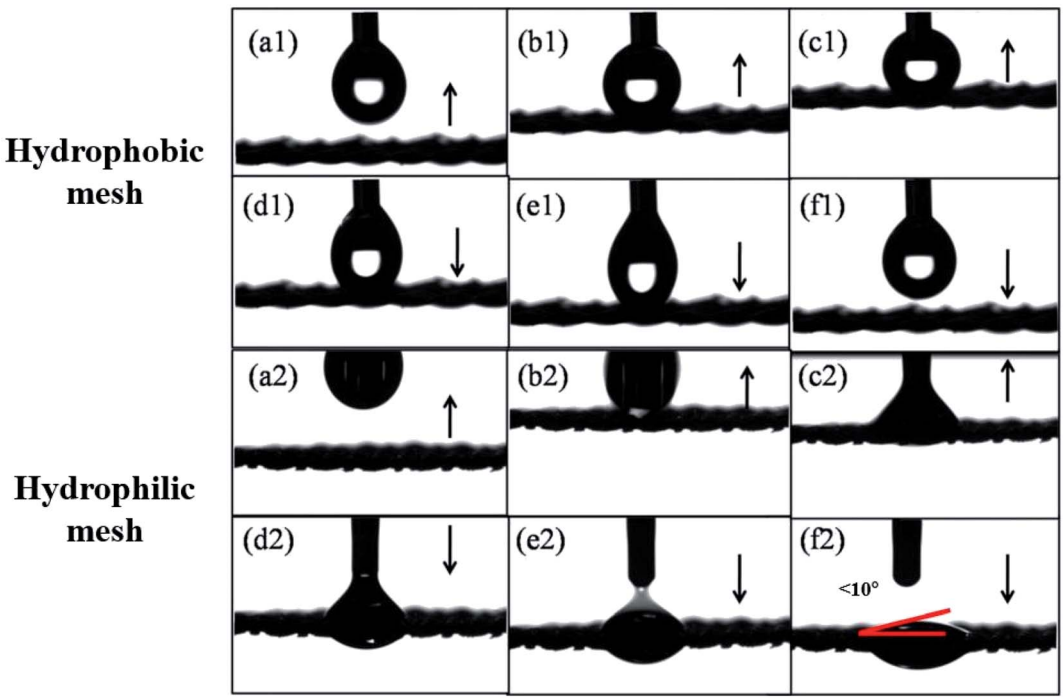

Fig. 3 Dynamic process of a water droplet in contact with the prepared hydrophobic and hydrophilic mesh surfaces. The arrows represent the direction of movement through the mesh. (a1)–(f1) and (a2)–(f2) Demonstrate the contact processes of the hydrophobic surface and the hydrophilic surface, respectively.

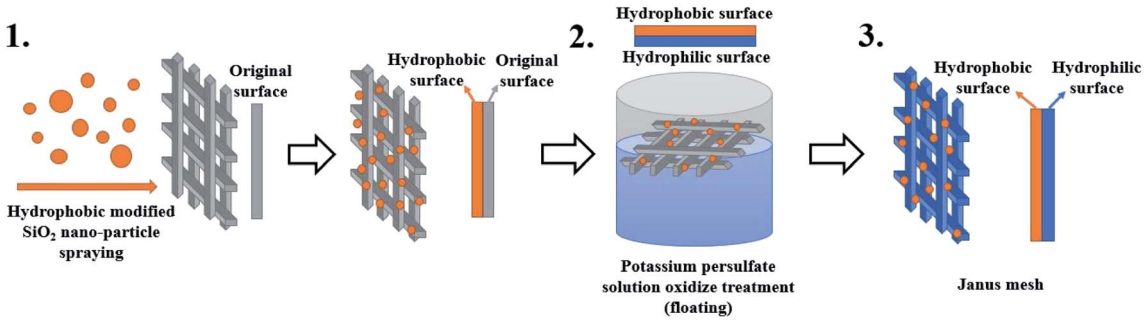

Fig. 4 A schematic diagram of the fabrication process of the Janus mesh for unidirectional water fluid transportation.

3.4 Unidirectional water transportation analysis

Water fluid unidirectional transportation of the as-prepared Janus mesh is demonstrated in Fig. 5. In our experiment, we placed the Janus mesh in a mock tube vertically in order to test its asymmetry blocking/passing properties. The water fluid will be blocked by the mesh when the water moves in a hydrophilic-to-hydrophobic direction, and this process is shown in Fig. 5(a)–(d). Fig. 5(a) shows the empty tube and Janus mesh system. The red arrows represent the direction of movement of the water fluid. Furthermore, in order to emphasize the location of the fluid, we used $CuSO_4$ to dye the water in this experiment. Fig. 5(b) shows that the water fluid movement from the hydrophilic side was blocked by the Janus mesh. Water was still blocked by the mesh when it carried on accumulating, as shown in Fig. 5(c). Finally, water fluid was still blocked even when the water nearly filled the tube, as shown in Fig. 5(d). The schematic diagrams are shown in Fig. 5(a1) and (b1). On the other hand, if the water fluid moves in a hydrophobic-to-hydrophilic direction, it can pass through the mesh freely. The process is demonstrated in Fig. 5(e)–(h). Water fluid comes from the hydrophobic side and goes to the hydrophilic side in the tube system, as shown in Fig. 5(e). Instead of being blocked by the mesh, the water fluid can pass easily through the mesh, as shown in Fig. 5(f). From Fig. 5(g) and (h), we can see that the water fluid carries on passing through the mesh as water accumulates. Using this novel phenomenon, the as-prepared Janus mesh can realize the unidirectional water transporting function. The corresponding schematic diagrams are shown in Fig. 5(c1) and (d1).

The unidirectional water blocking effect of a Janus membrane/mesh has been mentioned in a number of previous studies.[13,14,41] However, results from different articles appear to be rather confusing. Among the articles, a number of them have been similar to Yang's experiment.[14] Here, the authors used a hydrophilic cotton membrane as a substrate, and modified one side to be hydrophobic in order to fabricate a Janus membrane. The results showed that a water droplet could penetrate the membrane from the hydrophobic to the hydrophilic side, whilst be blocked in the opposite direction, and this is similar to our results. However, at the same time, there are

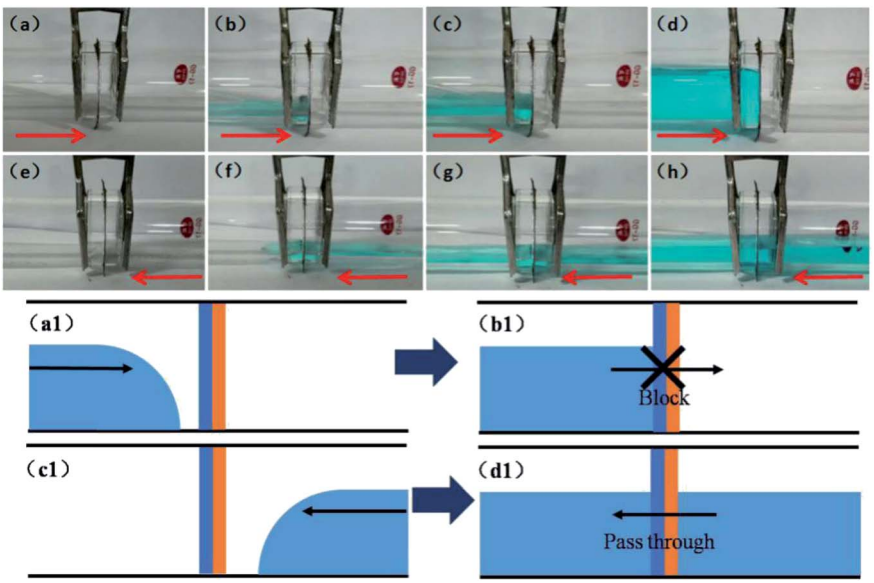

Fig. 5 Illustration of the unidirectional water fluid blocking/passing through function in a tube of the as-prepared Janus mesh. (a–h) show the actual images and (a1–d1) show the schematic diagram.

also many different results that are similar with Liu's experiment.[41] They used a hydrophobic polymer membrane as the substrate and conducted a hydrophilic modifying process on one side of the membrane to fabricate a Janus membrane. In the article, the membrane could block water fluid in two directions. However, when the hydrophilic side of the membrane was placed downwards and the hydrophobic side was placed upwards, the membrane could maintain a higher water column. It seems that the blocking effect is more intense in the hydrophobic-to-hydrophilic direction, and this is opposite to our results. Based on these previous works, we proposed a possible mechanism for the unidirectional blocking phenomenon of the Janus membrane. The mechanism diagram is shown in Fig. 6.

Fig. 6A shows a schematic diagram of our Janus mesh, and the picture on the right-hand side is the cross section of the mesh. We conducted hydrophobic nano SiO_2 particle spraying on one side of the substrate, and then utilized the etching effect of potassium persulfate solution to endow the substrate with hydrophilic property. Therefore, as the schematic graphic shows, our Janus mesh has a thick hydrophilic part and a thin hydrophilic part. Fig. 6B shows the passing process of water fluid that comes from the hydrophobic side and goes to the hydrophilic side. Fig. 6(b1) demonstrates the schematic graphic of the cross section. In Fig. 6(b2), we can see that the contact angle in the solid/liquid/gas three-phase point is rather large, and the surface free energy is extremely low at the hydrophobic part. The interface of the water forms a convex shape in the pores of the mesh. The Laplace pressure that is generated by the convex interface is in the reverse direction and has an impeding effect to the water fluid. However, the hydrophobic part of the mesh is so thin that the impeding effect cannot block the water fluid entirely. Water penetrates the hydrophobic part and comes into contact with the hydrophilic part of the mesh, as demonstrated in Fig. 6(b3). When the hydrophobic part is immersed entirely in water, the convex interface will not be formed and the reversed Laplace pressure disappears as well. On the other hand, a concave water interface can be formed at the hydrophilic part, and the Laplace pressure generated by the interface is in the forward direction. This phenomenon can have a positive effect for water fluid passing through the mesh. Under these circumstances, the impeding effect of the mesh comes inherently from the reversed pressure of the mesh pores. However, the effect cannot counterbalance the hydraulic pressure and forwards Laplace pressure that is generated from the assembled interface. Our experiment therefore indicates that the hydrophilic mesh cannot block the water fluid. Fig. 6(b4) shows that water fluid finally penetrates the pore of the mesh and Fig. 6(b5) shows the force analysis of this process.

Fig. 6C demonstrates that the process of water fluid moving in the hydrophilic-to-hydrophobic direction is blocked by the Janus mesh. The schematic graphic of the cross section is shown in Fig. 6(c1). In Fig. 6(c2), water fluid leaks into the pore and comes into contact with the hydrophilic part of the mesh. Pores of the mesh have an impeding effect to the water, but they cannot block the water fluid entirely. Therefore, water fluid moves forward and comes into contact with the hydrophobic part of the mesh, as shown in Fig. 6(c3). The convex water interface is formed in the pore and reversed Laplace pressure is generated simultaneously. In this case, impeding pressure is composed by inherent reversed pressure of the mesh pores and the reversed Laplace pressure. The two impeding effects can

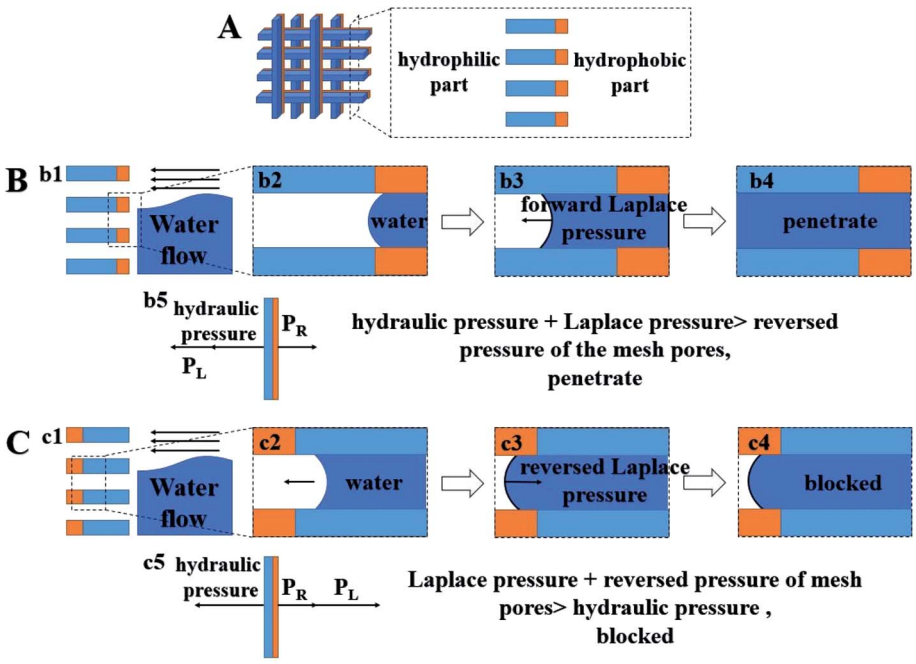

Fig. 6 The mechanistic diagram for the unidirectional blocking phenomenon of the Janus mesh. (A) Is the schematic graphic and cross section of the Janus mesh. B (b1–b4) shows the process of water fluid moving in the hydrophobic to hydrophilic direction and passing through the mesh. C (c1–c4) demonstrates the process of the water fluid moving from the hydrophilic to hydrophobic side and being blocked by the mesh.

overcome the hydraulic pressure so that the water fluid is blocked by the Janus mesh, as demonstrated in Fig. 6(c4). Fig. 6(c5) shows the force analysis of this process. Based on this theory, the unidirectional water blocking phenomenon of a "thick hydrophilic part and thin hydrophobic part" Janus membrane/mesh can be perfectly explained. As for the "thick hydrophobic part and thin hydrophilic part" Janus membrane/mesh, when water comes into contact with the hydrophobic part directly, it cannot penetrate the hydrophobic part of the mesh, so the water fluid is blocked. On the other hand, contacting the hydrophilic part first can help the water fluid pass through the mesh and reduces the impeding ability of the mesh. In summary, for a "thick hydrophobic part and thin hydrophilic part" Janus mesh, the blocking ability is more intense when water fluid comes from the hydrophobic side and goes to the hydrophilic side.

3.5 Analysis of the interface of the water fluid

When the Janus mesh is placed in a water tube, there is an interesting phenomenon of the water fluid that needs to be discussed, and this is described in Fig. 7. The interfaces of water behave differently at the two sides of the Janus mesh, and this phenomenon can be attributed to the difference in surface tension at the liquid/solid/gas three-phase points. For an integrated hydrophobic mesh, the interface of the water is in a convex shape. A schematic diagram is shown in Fig. 7(c1) and the actual image is shown in Fig. 7(c2). The water was dyed with $CuSO_4$ to display it more clearly. On the other hand, the interface of the water is in a concave shape if the mesh is integrated with hydrophilicity, as shown in Fig. 7(b1) and (b2). As for the Janus mesh with distinct wettability on its two sides, the interface of the water fluid also behaves differently at the two sides, as demonstrated in Fig. 7(a1) and (a2). On the hydrophobic side, the interface of the water fluid is in a convex shape, while on the hydrophilic side, the interface is in a concave shape. This novel phenomenon can be explained by the Young–Laplace equation. The interface of the water fluid is similar to a water droplet at the solid/liquid/gas three-phase point, as the well-known Young–Laplace equation demonstrates,

$$\gamma_{SG} - \gamma_{SL} = \gamma_{LG} \cos\theta \quad (3)$$

where γ_{SG}, γ_{LG} and γ_{SL} stand for the surface tensions of the solid–gas phase interface, the liquid–gas phase interface and of the solid–liquid phase interface. θ represents the contact angle of the droplet. The contact angle can be large for a hydrophobic surface, while it can be rather small for a hydrophilic surface, and this is shown by eqn (3). From the images, we can see that the convex interface at the hydrophobic side has a large contact angle. On the other hand, the concave interface at the hydrophilic side of the mesh has a small contact angle. This novel phenomenon fits Young's theory well.

In addition, for an as-prepared hydrophobic mesh surface, tiny water droplets may remain on the surface if they come into contact with the mesh first. The droplets that remain on the mesh can transform the hydrophobic surface into a hydrophilic one. Therefore, if a hydrophobic mesh blocks water fluid on one side first and then comes into contact with water again, the interface of the water can be different on two sides of the mesh, just as in a Janus mesh.

3.6 Stability of the prepared surface

The stability of a prepared mesh plays a vital role in its practical applications, as it determines the life span of the mesh. In order to evaluate the stability of the prepared Janus mesh in this work,

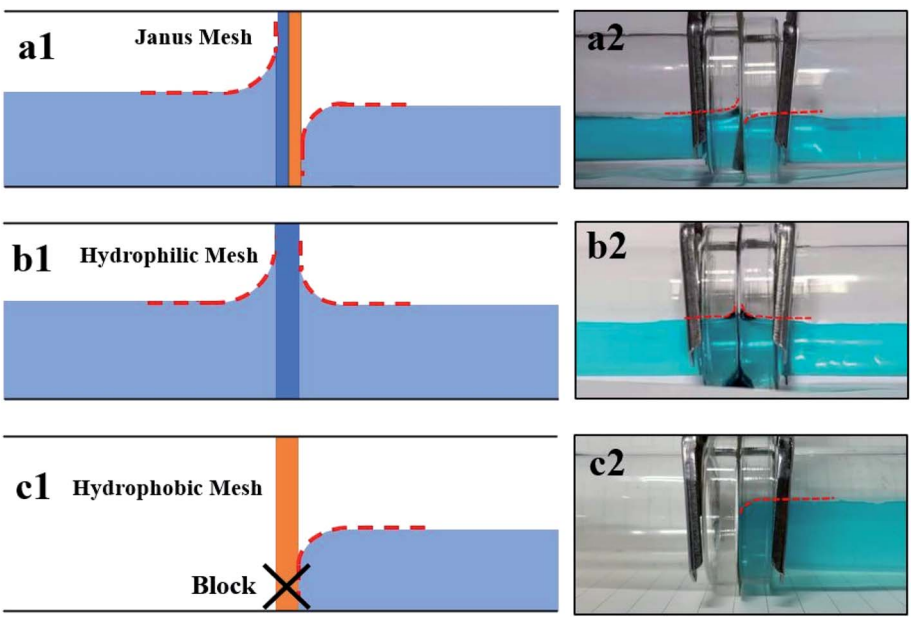

Fig. 7 Schematic diagram of the water fluid interface when in contact with the meshes with different wettability properties. (a1) and (a2) Show the water fluid surfaces of a Janus mesh. (b1) and (b2) Demonstrate the water fluid surfaces of a hydrophilic mesh, and (c1) and (c2) demonstrate the water fluid surfaces of a hydrophobic surface.

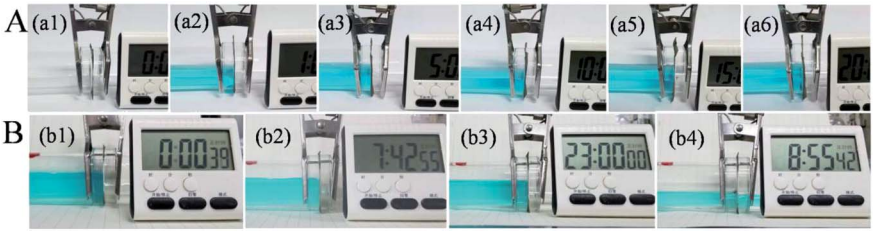

Fig. 8 Schematic diagram of the stability of the mesh. A (a1–a6) demonstrates the cycle times that the mesh can hold the water fluid and B (b1–b4) demonstrates the holding times that the mesh can maintain.

we tested the mesh from two aspects: the time it takes to hold the aqueous fluid stably (from the hydrophilic side to the hydrophobic side), and repeat circles of the mesh holding the water fluid (from the hydrophilic side to the hydrophobic side), as shown in Fig. 8.

As for the cycle times, the experimental results are shown in Fig. 8A. As mentioned above, the aqueous fluid can be blocked by the mesh when moving in a hydrophilic-to-hydrophobic direction, while it can penetrate the mesh when moving from the hydrophobic side to the hydrophilic side. In our experiment, we chose a Janus mesh with a mesh number of 200 as the specimen to test the unidirectional blocking stability of the mesh. We injected water fluid from the hydrophilic side to see if the mesh could block it. Then, we removed the mesh, dried it, and repeated the process again. Fig. 8(a1) demonstrates the testing system. The display device next to the tube showed the cycle number that the mesh had been tested. As Fig. 8(a2)–(a6) show, the mesh could block the fluid after 1, 5, 10, 15 and 20 cycles, and so the mesh showed outstanding stability. It is also worth mentioning that during the stability experiment, water fluid could pass through the mesh in the hydrophobic-to-hydrophilic direction, maintaining its unidirectional blocking function in the process.

When it came to the amount of time holding the aqueous fluid, the prepared Janus mesh also showed excellent stability. The testing process of the prepared Janus mesh is demonstrated in Fig. 8B. The clock in the image shows the time the mesh held the water fluid. The maximum number of the clock is 24 h. Fig. 8B(b1)–(b3) show that the Janus mesh could hold water without any leaking. After 32 h, water fluid finally leaked from the mesh, as (b4) shows. The results indicate good stability of the prepared mesh, greatly expanding its application potential.

It is clear that, compared with static fluid, the collision effect between a stream current and the mesh can help the water to penetrate the Janus mesh. Our experiments also confirmed this point. The "Reynold numbers" factor contains the influence of varying viscosities and different diameters, and is the ideal factor for measuring the effect of a moving stream current. In our experiment, we adjusted the rate of the water flow and maintained the other factors in order to change the Reynold numbers of the aqueous fluid. The as-prepared Janus mesh could hold static water from the hydrophilic side to the hydrophobic side. For a moving water current, the mesh could hold water when the velocity of the fluid was slow. As we gradually increased the velocity, the moving water current finally passed through the mesh. The equation used to calculate the Reynold number is demonstrated as follows:

$$\mathrm{Re} = \frac{\rho v d}{\mu}$$

where Re, ρ, v, d, and μ stand for the Reynold number, density of the liquid, the velocity of the flow, diameter of the tube and the viscosity of the liquid, respectively. In our experiment, the diameter of the tube was fixed at 5 micrometer, and the temperature of the environment was 20 °C. Under these circumstances, the viscosity of the water was 1.0050 mPa s. The aqueous fluid could penetrate the as-prepared Janus mesh when the velocity of the flow was larger than 0.90 m s^{-1}. The results of our experiment are shown in the following table (Table 2).

The experiment confirms that the collision between the fluid and the mesh can help the water to penetrate the mesh. At the same time, the as-prepared mesh also demonstrated outstanding stability when blocking the stream current unidirectionally.

As for the phenomenon of "leaking after 32 h", we have proposed a theory to explain it. We conducted facile modification of the surface of the mesh to endow the surfaces with different wettability properties. However, as mentioned above, tiny droplets that remain on the surface can transform a hydrophobic surface into a hydrophilic one. During the stability test, water vapor could penetrate the holes of the mesh from the hydrophilic side and condense on the hydrophobic side, changing the wettability of the hydrophobic surface. After 32 hours, the mesh loses its Janus wettability and transforms into a hydrophilic one that can hardly hold the water fluid. In this case, water fluid can pass through the mesh, as demonstrated by the experiment.

Table 2 The Reynold numbers and other factors of the stream current test

V (m s^{-1})	ρ (kg m^{-3})	μ (mPa s)	T (°C)	d (mm)	Re	Pass or blocked
0.90	1000	1.0050	20	5	4477.6	Pass
0.77					3837.9	Blocked
0.64					3198.3	Blocked
0.51					2558.6	Blocked
0.26					1279.3	Blocked

4. Conclusion

In this work, we endowed a copper mesh substrate with opposite wettability on its two sides in order to fabricate a mesh with Janus wetting properties. We utilized potassium persulfate solution to oxidize one side of the mesh to fabricate hydrophilicity and sprayed hydrophobic-modified SiO_2 nanoparticles onto the other side to fabricate hydrophobicity. We sprayed one side of the mesh first and then floated the mesh on the interface of potassium persulfate solution so that the hydrophobic side could be kept away from the etching process. The prepared mesh could transport water fluid unidirectionally. Water passed through the mesh in the hydrophobic-to-hydrophilic direction, while it was blocked in the opposite direction. The possible principle for this based on force analysis is discussed in this work and the stability was recorded as being good enough. The interesting phenomenon in the way that the interface of the water fluid behaves was also discussed. The prepared Janus mesh has great potential in medical fields, energy fields and in the chemistry industry.

Author contributions

All authors contributed to the development of the experimental design and discussion of the results, as well as to the preparation of the manuscript. All authors have given approval to the final version of the manuscript.

Conflicts of interest

There are no conflicts to declare.

Acknowledgements

The authors are extremely grateful to the support from the National Natural Science Foundation of China (grant no. 21802004 and no. 51971012) and the National Key Research and Development Program (2018YFB2002000).

References

1 B. Su, Y. Tian and L. Jiang, Bioinspired interfaces with superwettability: from materials to chemistry, *J. Am. Chem. Soc.*, 2016, **138**(6), 1727–1748.
2 D. Li, J. Huang, G. Han, *et al.*, A facile approach to achieve bioinspired PDMS@ Fe_3O_4 fabric with switchable wettability for liquid transport and water collection, *J. Mater. Chem. A*, 2018, **6**(45), 22741–22748.
3 H. Chen, T. Ran, Y. Gan, *et al.*, Ultrafast water harvesting and transport in hierarchical microchannels, *Nat. Mater.*, 2018, **17**(10), 935–942.
4 J. Lin, X. Tan, T. Shi, *et al.*, Leaf vein-inspired hierarchical wedge-shaped tracks on flexible substrate for enhanced directional water collection, *ACS Appl. Mater. Interfaces*, 2018, **10**(51), 44815–44824.
5 M. Z. Khan, V. Baheti, J. Militky, *et al.*, Superhydrophobicity, UV protection and oil/water separation properties of fly ash/trimethoxy (octadecyl) silane coated cotton fabrics, *Carbohydr. Polym.*, 2018, **202**, 571–580.
6 S. C. Koşak, S. Trosien and M. Biesalski, Superhydrophobic hybrid paper sheets with Janus-type wettability, *ACS Appl. Mater. Interfaces*, 2018, **10**(43), 37478–37488.
7 H. Ye, L. Zhu, W. Li, *et al.*, Simple spray deposition of a water-based superhydrophobic coating with high stability for flexible applications, *J. Mater. Chem. A*, 2017, **5**(20), 9882–9890.
8 K. M. Lee, H. Park, J. Kim, *et al.*, Fabrication of a superhydrophobic surface using a fused deposition modeling (FDM) 3D printer with poly lactic acid (PLA) filament and dip coating with silica nanoparticles, *Appl. Surf. Sci.*, 2019, **467**, 979–991.
9 X. Wang, J. Zeng, X. Yu, *et al.*, Water harvesting method *via* a hybrid superwettable coating with superhydrophobic and superhydrophilic nanoparticles, *Appl. Surf. Sci.*, 2019, **465**, 986–994.
10 J. Sun, C. Chen, J. Song, *et al.*, A universal method to create surface patterns with extreme wettability on metal substrates, *J. Colloid Interface Sci.*, 2019, **535**, 100–110.
11 G. Li, Z. Zhang, P. Wu, *et al.*, One-step facile fabrication of controllable microcone and micromolar silicon arrays with tunable wettability by liquid-assisted femtosecond laser irradiation, *RSC Adv.*, 2016, **6**(44), 37463–37471.
12 H. Qian, J. Yang, Y. Lou, *et al.*, Mussel-inspired superhydrophilic surface with enhanced antimicrobial properties under immersed and atmospheric conditions, *Appl. Surf. Sci.*, 2019, **465**, 267–278.
13 H. C. Yang, Y. Xie, J. Hou, *et al.*, Janus membranes: creating asymmetry for energy efficiency, *Adv. Mater.*, 2018, **30**(43), 1801495.
14 X. Yang, L. Yan, F. Ran, *et al.*, Interface-confined surface engineering constructing water-unidirectional Janus membrane, *J. Membr. Sci.*, 2019, **576**, 9–16.
15 P. Gupta and B. Kandasubramanian, Directional fluid gating by janus membranes with heterogeneous wetting properties for selective oil–water separation, *ACS Appl. Mater. Interfaces*, 2017, **9**(22), 19102–19113.
16 X. Lin, J. Heo, M. Choi, *et al.*, Simply realizing durable dual Janus superwettable membranes integrating underwater low-oil-adhesive with super-water-repellent surfaces for controlled oil–water permeation, *J. Membr. Sci.*, 2019, **580**, 248–255.
17 J. Wang, F. Han, Y. Chen, *et al.*, A pair of MnO_2 nanocrystal coatings with inverse wettability on metal meshes for efficient oil/water separation, *Sep. Sci. Technol.*, 2019, **209**, 119–127.
18 Q. Li, B. Yu, F. Guo, L. Cao and X. Yi, Effect of Cr_3C_2 Addition on Properties of ZrB_2-SiC Ceramic, *J. Mater. Eng.*, 2018, **46**(12), 78–84.
19 X. Yue, Z. Li, T. Zhang, *et al.*, Design and fabrication of superwetting fiber-based membranes for oil/water separation applications, *Chem. Eng. J.*, 2019, **364**, 292–309.
20 N. Wang, Y. Zhai, Y. Yang, *et al.*, Electrostatic assembly of superwetting porous nanofibrous membrane toward oil-in-

water microemulsion separation, *Chem. Eng. J.*, 2019, **354**, 463–472.

21 Z. S. Huang, Y. Y. Quan, J. J. Mao, *et al.*, Multifunctional superhydrophobic composite materials with remarkable mechanochemical robustness, stain repellency, oil-water separation and sound-absorption properties, *Chem. Eng. J.*, 2019, **358**, 1610–1619.

22 H. K. Raut, A. S. Ranganath, A. Baji, *et al.*, Bio-inspired hierarchical topography for texture driven fog harvesting, *Appl. Surf. Sci.*, 2019, **465**, 362–368.

23 P. Zhao, N. Qin, L. Carolyn, *et al.*, Polyamide 6.6 separates oil/water due to its dual underwater oleophobicity/underoil hydrophobicity: role of 2D and 3D porous structures, *Appl. Surf. Sci.*, 2019, **466**, 282–288.

24 Y. Liang, S. Kim, P. Kallem, *et al.*, Capillary effect in Janus electrospun nanofiber membrane for oil/water emulsion separation, *Chemosphere*, 2019, **221**, 479–485.

25 C. Yao, M. Luo, H. Wang, *et al.*, Asymmetric wetting Janus fabrics with double-woven structure for oil/water separation, *J. Mater. Sci.*, 2019, **54**(7), 5942–5951.

26 Y. Y. Kong and J. H. Xin, Janus Fabric with Self-Propelled Directional Wetting Patterns Induced by Light and Temperature, *Adv. Eng. Mater.*, 2018, **20**(8), 1700905.

27 X. Chen, J. Xu, D. Sun, *et al.*, Emulsion interfacial synthesis of polymer/inorganic Janus particles, *Langmuir*, 2019, **35**(18), 6032–6038.

28 X. Mao, L. Gong, L. Xie, *et al.*, Novel Fe_3O_4 based superhydrophilic core-shell microspheres for breaking asphaltenes-stabilized water-in-oil emulsion, *Chem. Eng. J.*, 2019, **358**, 869–877.

29 N. Wang, Y. Wang, B. Shang, *et al.*, Bioinspired one-step construction of hierarchical superhydrophobic surfaces for oil/water separation, *J. Colloid Interface Sci.*, 2018, **531**, 300–310.

30 Y. Zhao, C. Yu, H. Lan, *et al.*, Improved interfacial floatability of superhydrophobic/superhydrophilic Janus sheet inspired by lotus leaf, *Adv. Funct. Mater.*, 2017, **27**(27), 1701466.

31 C. Xu, H. Liu, W. Liang, *et al.*, Creating gradient wetting surfaces *via* electroless displacement of zinc-coated carbon steel by nickel ions, *Appl. Surf. Sci.*, 2018, **434**, 940–949.

32 W. Liang, L. Zhu, C. Xu, *et al.*, Facile fabrication of antiwax conversion coatings based on water film theory, *Mater. Lett.*, 2016, **176**, 56–59.

33 W. Liang, L. Zhu, W. Li, *et al.*, Facile fabrication of binary nanoscale interface for no-loss microdroplet transportation, *Langmuir*, 2016, **32**(22), 5519–5525.

34 W. Liang, L. Zhu, C. Xu, *et al.*, Ecologically friendly conversion coatings with special wetting behaviors for wax prevention, *RSC Adv.*, 2016, **6**(31), 26045–26054.

35 W. Liang, L. Zhu, W. Li, *et al.*, Facile fabrication of a flower-like CuO/Cu $(OH)_2$ nanorod film with tunable wetting transition and excellent stability, *RSC Adv.*, 2015, **5**(48), 38100–38110.

36 W. Liang, L. Zhu, W. Li, *et al.*, Bioinspired composite coating with extreme underwater superoleophobicity and good stability for wax prevention in the petroleum industry, *Langmuir*, 2015, **31**(40), 11058–11066.

37 E. J. Lee, B. J. Deka and A. K. An, Reinforced superhydrophobic membrane coated with aerogel-assisted polymeric microspheres for membrane distillation, *J. Membr. Sci.*, 2019, **573**, 570–578.

38 K. Sasaki, M. Tenjimbayashi, K. Manabe, *et al.*, Asymmetric superhydrophobic/superhydrophilic cotton fabrics designed by spraying polymer and nanoparticles, *ACS Appl. Mater. Interfaces*, 2016, **8**(1), 651–659.

39 X. Xue, C. Yu, J. Wang, *et al.*, Superhydrophobic cones for continuous collection and directional transportation of CO_2 microbubbles in CO_2 supersaturated solutions, *ACS Nano*, 2016, **10**(12), 10887–10893.

40 X. Liu, J. Gao, Z. Xue, *et al.*, Bioinspired oil strider floating at the oil/water interface supported by huge superoleophobic force, *ACS Nano*, 2012, **6**(6), 5614–5620.

41 Y. Liu, R. Qu, W. Zhang, *et al.*, Lotus-and mussel-inspired PDA–PET/PTFE Janus membrane: toward integrated separation of light and heavy oils from water, *ACS Appl. Mater. Interfaces*, 2019, **11**(22), 20545–20556.